JOURNAL OF AIRCRAFT
Vol. 33, No. 5, September–October 1996

Experimental Measurements of Dynamic Control Surface Effectiveness

R. M. Rennie* and E. J. Jumper†
University of Notre Dame, Notre Dame, Indiana 46556

This article reports on a low Reynolds number experimental study of the unsteady lift characteristics of an NACA 0009 airfoil pitched about its midchord, equipped with a 27% trailing-edge flap that could be independently deflected. The airfoil normal force, obtained from integrated surface pressure measurements, was captured during rapid, trailing-edge flap-only deflections; rapid, arbitrary, pitch-only excursions; and combined rapid pitch and flap-deflection motions. The measured aerodynamic response of the flapped airfoil to the various flap, airfoil, and airfoil–flap combination motions was compared to theoretical and panel-code-computed aerodynamic-response predictions. These comparisons, and the results of flow visualization experiments, led to the observation that both the flap's effectiveness and the airfoil's lift–curve slope were higher during their motion than their steady-state values, and essentially matched their inviscid theoretical values.

Nomenclature

a_1 = flap coefficient, $\cos^{-1}e - e\sqrt{1-e^2}$
a_2 = flap coefficient, $\frac{1}{3}\sqrt{1-e^2}(2+e^2) - e\cos^{-1}e$
a_3 = flap coefficient, $\cos^{-1}e(1-2e) + \sqrt{1-e^2}(2-e)$
a_4 = flap coefficient, $2\sqrt{1-e^2} + 2\cos^{-1}e$, inviscid value
b = airfoil semichord, $c/2$
C_l = lift coefficient
$C_{l_{ss}}$ = steady-state lift coefficient
$C_{l\alpha}$, $C_{n\alpha}$ = C_l, C_n vs α lift–curve slope
$C_{l\delta_{TE}}$, $C_{n\delta_{TE}}$ = C_l, C_n vs δ_{TE} lift–curve slope
C_n = normal force coefficient
c = airfoil chord
e = distance from airfoil midchord to flap hinge, nondimensionalized by b
Re = Reynolds number
s, σ = nondimensional time, tV_∞/b
t = time
V_∞ = freestream velocity
α = angle of attack
δ_{TE} = trailing-edge flap deflection angle
$\dot{\delta}_{TE}$ = nondimensional trailing-edge flap deflection rate, $\dot{\delta}^*_{TE}b/V_\infty$
$\ddot{\delta}_{TE}$ = nondimensional trailing-edge flap angular acceleration, $\ddot{\delta}^*_{TE}b^2/V_\infty^2$
τ = flap effectiveness factor
$\phi(s)$ = Wagner function, $\simeq(s+2)/(s+4)$

Superscript
* = dimensional quantities

I. Introduction

OVER the last decade, there has been a renewed emphasis on enhancing the maneuverability of fighter aircraft; this enhancement was initially referred to as supermaneuverability.[1] Supermaneuverability is associated with both increasing maximum C_l, through possible exploitation of unsteady aerodynamic phenomena like dynamic stall,[2] and improving aircraft agility. Agility, as defined by Skow,[3] refers to the ability to quickly point an aircraft, control its trajectory and shorten its transition time between maneuvers. While specific maneuvers associated with agility might depend on high C_l, agility need not imply high C_l; it is often the case that agility implies the suppression of lift. Such suppression, for example, would be required to rapidly point an aircraft fuselage (and thus the wing angle of attack) while independently controlling or maintaining the aircraft trajectory. In steady flow, independent control of airfoil angle of attack and lift can be accomplished by concomitant trailing-edge flap deflections. Our specific research has investigated the use of trailing-edge flaps to control lift during dynamic pitch motions of the airfoil, where the lift histories associated with angle-of-attack changes and flap deflections are sufficiently rapid that both must be treated as unsteady.

The unsteady aerodynamic response for trailing-edge flap motions has been investigated theoretically,[4–7] and to a more limited extent, experimentally.[8–10] Airfoil lift characteristics for unsteady trailing-edge flap motions were first analyzed by Theodorsen[4] for harmonically oscillating flaps. As in the case of unsteady airfoil motions, Theodorsen's results for oscillating trailing-edge flaps can be generalized to arbitrary flap motions using the method of Jones[5] and others,[6–8] and can be expressed as

$$C_l = a_1\dot{\delta}_{TE} + a_2\ddot{\delta}_{TE} + \int_0^s (a_4\dot{\delta}_{TE} + a_3\ddot{\delta}_{TE})\phi(s-\sigma)\,d\sigma \quad (1)$$

The term representing the circulatory lift caused by impulsive start has been omitted from Eq. (1). Attempts to experimentally validate Eq. (1) for arbitrary motions have been few. References 9 and 10 present recent experimental data on unsteady flap motions, but treat small-amplitude oscillatory motions at compressible flow speeds only. Of particular note, however, is

Presented as Paper 94-0504 at the AIAA 32nd Aerospace Sciences Meeting and Exhibit, Reno, NV, Jan. 10–13, 1994; received April 21, 1995; revision received April 30, 1996; accepted for publication May 7, 1996.

*Graduate Assistant, Hessert Center for Aerospace Research, Department of Aerospace and Mechanical Engineering; currently Aerodynamicist, Aiolos Engineering Corporation, 51 Constellation Court, Suite 200, Toronto, Ontario L5N 2S6, Canada. Student Member AIAA.

†Associate Professor, Hessert Center for Aerospace Research, Department of Aerospace and Mechanical Engineering. Associate Fellow AIAA.

the work of Drescher,[8] who used a 30-cm, Gö-409 airfoil with a 9-cm, simple-hinged, trailing-edge flap in a (1 × 0.728 m test section) water tunnel ($Re \simeq 1 \times 10^6$), and was able to achieve nondimensional flap rates from 0.01 to 0.5. Drescher studied a variety of flap motions, reporting on both sinusoidal and ramp motions. Using 21 symmetrically placed surface pressure taps, he was able to capture integrated lift histories, which he compared to an arbitrary-flap-motion lift theory developed by Küssner and Schwarz.[6]

The use of trailing-edge flaps as unsteady lift-control devices has been investigated for the suppression of flutter[11-15] and for gust alleviation.[13,16] Hugo and Jumper[17] reported on an incompressible, unsteady lift-control study to cancel the effect of a gust or control the lift on an airfoil caused by arbitrary, dynamic angle-of-attack changes. Linearized, unsteady-airfoil theory for arbitrary flap motions was used to arrive at a lift-control algorithm, which was successfully tested using an inviscid, unsteady panel code. Although the panel code was inviscid, it accounted for airfoil thickness, true flap deflection (i.e., the boundary condition of no-flow through the flap surface was used), and a deformable wake, so that the computed lift results were nonlinear; in the numerical study, the linearized lift-control algorithm appeared to successfully control lift during angle-of-attack changes, as well as cancel (alleviate) the lift caused by the convection of a relatively large vortical gust past the airfoil.

The lift-control algorithm[17] referred to earlier was investigated experimentally in a series of low Reynolds number experiments ($Re \simeq 2 \times 10^5$). These studies were divided into three parts: in the first part, the airfoil's unsteady lift response caused by flap motions only was investigated; in the second part, the airfoil's unsteady lift response caused by changes in angle of attack about the midchord was investigated; and finally, a series of experiments was performed that combined angle-of-attack changes with algorithm-prescribed flap motions in an attempt to control to zero lift. As will be argued, these studies suggested that the airfoil's unsteady lift response to both flap and airfoil motions was well represented by unsteady, inviscid theory while the flap or airfoil were in motion. Once the motion ended the lift response decayed and could no longer be described by inviscid theory.

II. Experimental Approach

A. Apparatus

Experimental data were collected in the University of Notre Dame subsonic wind tunnel, which is an indraft configuration that features 2 × 2 ft cross-sectional, interchangeable test sections. To prevent fan disturbances from propagating upstream into the test section, a 6-ft-long constant area duct (2 × 2 ft cross section), followed by a straw box was inserted between the test section and the diffuser; with this configuration, the maximum attainable test-section velocity was 45 ft/s. The mean test-section turbulence level with this setup was less than 0.04%.

A test section consisting of a frame, airfoil, and motion control hardware was designed and constructed as shown schematically in Fig. 1. The airfoil used in the study was an NACA 0009 profile of 8-in. chord with a 20% leading-edge flap and a 27% trailing-edge flap, both of which were a simple-hinged type. In all of the tests reported here, the leading-edge flap was fixed at 0-deg deflection. The airfoil was instrumented with 36 surface pressure taps, each of which was connected to a 2 ft length of 0.05-in.-i.d. plastic pressure tubing. More complete descriptions of the experimental apparatus are given in Refs. 18 and 19.

B. Data Acquisition

Pressure data were acquired using either a single pressure transducer attached to a scanivalve for static experiments, or multiple pressure transducers for dynamic experiments. The pressure transducers used for both static and dynamic experiments had a pressure range of ±0.35 psig and a dynamic range on the order of 50 kHz, well beyond the requirements of the investigation. All 36 taps were used for static data; however, because the data acquisition system[19] could only acquire time series for 14 unsteady pressure signals and one position signal during a single dynamic experimental run, unsteady experiments used 28 taps. A single, complete, 28-tap, experimental data set required a minimum of two runs, one for each of two 14-tap sets. Up to 10 complete 28-tap data sets were acquired for each dynamic experiment (i.e., 20 runs, 10 for the first 14-tap set and 10 for the second 14-tap set), and these data sets were ensemble-averaged prior to reduction. The same taps were used for all experiments and are shown in Fig. 2, where the circled taps in Fig. 2 were excluded for dynamic testing. The use of 28 pressure taps on the airfoil for dynamic testing is similar to the number used by other investigators.[2,8,20,21] The position signal measurements were used for either the trailing-edge flap deflection history or the airfoil angle-of-attack history.

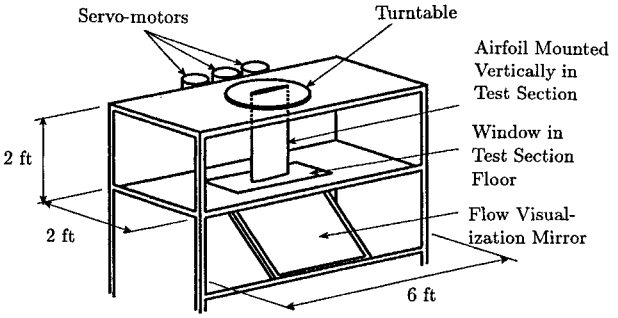

Fig. 1 Drawing of test section showing major components.

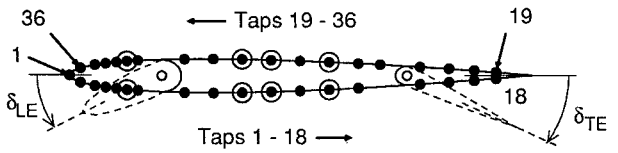

Fig. 2 Pressure tap locations. Circled taps were excluded from dynamic experiments.

C. Dynamic Response of Plastic Pressure Tubing

An important consideration in the method used to measure dynamic airfoil surface pressures was the effect that the 30 in. (2 ft inside the airfoil plus 6 in. of added slack) of 0.05-in.-i.d. plastic pressure tubing (connecting the surface taps to the pressure transducers) had on the unsteady pressure signals. This effect was investigated in an independent experiment similar to that of Ref. 22. An unsteady pressure signal consisting of 50-Hz bandwidth pseudorandom noise was created by mechanically driving a speaker diaphragm through large excursions using a signal generator. The speaker formed one end of a cylindrical pressure vessel; in the opposite end were two small, closely spaced holes. A pressure transducer (transducer A) was mounted into one of the holes, and the other hole was connected to a second transducer (transducer B) through one of the 30-in. plastic tubes. The time-domain output of each transducer was Fourier transformed, and the transfer function of the pressure tubing was computed. For a complete description of the technique, the reader is referred to Ref. 19. The transfer function for each tap showed that the pressure tubing had little effect on the amplitude of unsteady pressure signals up to a frequency of approximately 25 Hz, and that the phase lag caused by the tubing varied linearly with frequency up to around 40 Hz. This linear variation of phase lag with frequency demonstrated that the effect of the pressure tubing was a simple constant time delay on all pressure signals with frequency components below 25 Hz. This time delay was mea-

sured to be 5 ms (millisecond), and was removed from the pressure signals by correcting the time histories for all pressure data.

D. Data Reduction

For dynamic experiments, the pressure signals (and one position signal) were sampled in a serial fashion so that, depending on the motion rates involved, the airfoil or flap could move up to a maximum of 0.5 deg (for the maximum rates used) between the start and finish of a complete data scan. The 5-ms delay-corrected data were therefore adjusted to a common instant in time by linearly interpolating the signals closest to the time of interest. The chord-normal aerodynamic coefficient C_n was then calculated by numerically integrating the measured pressure distribution about the airfoil contour:

$$C_n = \oint C_p \, \mathrm{d}\left(\frac{x}{c}\right) \tag{2}$$

For experiments involving motion of the flap, the chord-normal coefficient of the flap was adjusted to the chord-normal direction of the main airfoil section:

$$C_{n_{\text{flap}}} = \oint_{\text{flap}} C_p \, \mathrm{d}\left(\frac{x_{\text{flap}}}{c}\right) \cos \delta_{\text{TE}} - \oint_{\text{flap}} C_p \, \mathrm{d}\left(\frac{y_{\text{flap}}}{c}\right) \sin \delta_{\text{TE}} \tag{3}$$

The pressure at the airfoil trailing edge was estimated by averaging the two pressures measured at the two taps closest to the airfoil trailing edge on the upper and lower surfaces of the airfoil. For experiments involving motion of the flap only, the airfoil was fixed at 0-deg angle of attack, so that the airfoil lift coefficient was identical to the airfoil normal force coefficient ($C_l = C_n$). For experiments involving pitch motions of the airfoil, the maximum airfoil angle of attack was 7 deg. Rather than converting C_n measurements to C_l, all data were reported as C_n. The static, wind-tunnel wall blockage correction to the lift coefficient for a 10-deg flap deflection was calculated, following the procedure outlined in Ref. 23 to be less than 4%. Blockage corrections were neglected, since it was expected that the unsteady blockage would be even lower than this static value.

The error associated with the integrated C_n data can be divided into random error and systematic error. For a typical ensemble-averaged data set the standard deviation in C_n was measured to be 0.007. An attempt was made to minimize systematic errors by calibrating the pressure transducers prior to each series of runs. The variation in transducer calibration–curve slope between calibrations was never found to be more than 0.2%. However, the variation in the transducer calibration–curve intercept values was an order of magnitude larger, and it was found that this error of the intercept values introduced a small error into the pressures measured for each tap, that was essentially constant over the time duration of an experimental run. These pressure (or C_p) errors enclosed a finite area in the airfoil C_p distribution so that, when the C_p distribution was integrated to determine C_n, the small errors introduced by the transducer–calibration intercept errors resulted in a constant offset in the C_n at each measurement time. This offset was removed from the C_n data by subtracting (i.e., taring) the C_n measured at zero angle of attack and zero flap deflection from the C_n values measured during the subsequent motion. The technique employed for the removal of the effect of the transducer intercept errors from the individual C_p measurements is discussed later.

III. Results

A. Flap Static Lift Measurements

Measurement of the static C_n vs δ_{TE} curve was performed using a scanivalve to sample all 36 pressure taps on the airfoil.

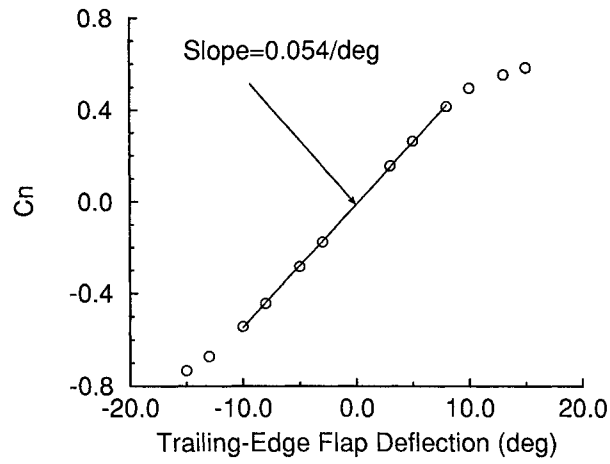

Fig. 3 Static C_n vs δ_{TE}.

Because only a single pressure transducer was used, every pressure measurement had exactly the same intercept error. The static C_n values, therefore, did not require a tare adjustment, since the integrated effect [i.e., Eq. (2)] of the pressure measurement intercept errors canceled. The coefficient C_n is plotted as a function of δ_{TE} in Fig. 3. Although not shown here, the integrated C_n vs δ_{TE} data were also compared to the C_n vs δ_{TE} from a force balance for an NACA 0009, 27% trailing-edge-flapped wing; these force-balance-derived C_n data matched, within experimental error, the results of Fig. 3. The wing used in the force balance measurements was mounted between two wall plates that were displaced 2 in. from the wind-tunnel floor and roof, and projected 1 ft in front of the wing. The static C_n vs δ_{TE} curve is approximately linear for flap deflections in the range of ± 10 deg; however, Fig. 3 shows a noticeable decline in the effectiveness of the flap for positive flap deflections above ~8 deg. This reduction in flap effectiveness at positive deflections was probably caused by a slight offset in the flap hinge location, resulting in imperfect aerodynamic blending of the flap with the main airfoil section at positive flap deflections. A linear least-squares fit to the C_n vs δ_{TE} curve for flap deflections in the range -10 deg $\leq \delta_{\text{TE}} \leq 8$ deg gave a slope ($C_{n\delta_{\text{TE}}}$) of 0.054/deg; the corresponding slope from steady airfoil theory is 0.0691/deg. A C_n vs δ_{TE} curve using the 28 pressure taps used in the unsteady experiments essentially duplicated the 36-tap curve shown in Fig. 3. Note that, although these results were obtained at low Reynolds number, the flap lift–curve slope of 0.054/deg is consistent with experimental values measured at high Reynolds number for the same airfoil and flap configuration.[24]

B. Flap Dynamic Lift Measurements

Dynamic flap–ramp motions, in the form of a constant-angular-rate ramp to the maximum flap deflection, were performed at angular rates ranging from 25 to 300 deg/s. These rates, at a tunnel velocity of 45 ft/s ($Re = 2 \times 10^5$), corresponded to nondimensional ramp rates $\dot{\delta}_{\text{TE}}$ of 0.003–0.039. For all flap–ramp experiments, the airfoil was maintained at 0-deg angle of attack throughout the run, and the flap was started from an initial deflection of 0 deg.

The measured unsteady lift and flap deflection histories for a typical flap–ramp experiment, for which the tunnel velocity was 45 ft/s, the flap rotation rate was 200 deg/s, and the final flap deflection angle was 10 deg, are shown in Fig. 4; this tunnel velocity and flap rotation rate corresponded to a nondimensional rate $\dot{\delta}_{\text{TE}}$ of 0.026. At this flap-deflection rate, and using a 300 scan/s data acquisition rate, it was possible to acquire 15 complete scans of the 28-tap pressure distribution on the airfoil while the flap was in the process of moving from 0 to 10 deg. As discussed earlier in Sec. II.B, the experimental unsteady lift history shown in Fig. 4 is the average of 10 com-

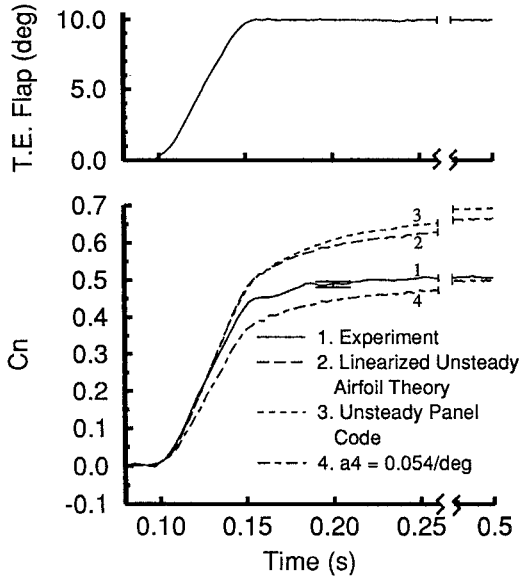

Fig. 4 Comparison of experimental unsteady lift history with inviscid models for $\delta_{TE} = 0.023$.

posite lift histories, compiled from 20 flap–ramp runs (10 for each of two sets of 14 pressure taps). As seen in Fig. 4, noise is present on the experimental lift history; this noise, and the random error associated with the measurement, is characterized by the error bar that denotes the precision interval (92% confidence) for the finite number of 10 lift measurements made at each instant in time. It should be noted that the experimental C_n history in Fig. 4 was adjusted (tared) to zero at the starting time when the flap was at a steady 0-deg deflection. This tare was subtracted from all subsequent values of C_n in the data set. Except for the subtracted tare, the data in Fig. 4 is presented as is, that is, no postprocessing routines were used to smooth the data.

C. Comparison of Experimental Unsteady Lift Histories with Computed Predictions

Experimental results were compared to unsteady airfoil theory [Eq. (1)] and to the results from the unsteady panel code[17] referred to earlier. The unsteady panel code was based on a Smith and Hess[25] method, and extended to the unsteady case using the Basu and Hancock[26] implementation of the unsteady Kutta condition. The wake was modeled using discrete, point vortices, which were allowed to convect at the local flow velocity; the code thus featured a deforming wake. This code has been shown to closely mimic unsteady airfoil theory for very thin airfoils at rates exceeding those used in our experiments. Thus, as mentioned previously, the code accounted for thickness, true flap deflection, and a deformable wake, without resorting to linearization; the code did not, however, account for viscosity.

Both the unsteady airfoil theory and the panel code results shown in Fig. 4 (second and third curves, respectively), were computed using the measured flap-motion history for the experiment. Two observations can be made from Fig. 4. The first is that the output of the unsteady panel code compares well to that of the linearized unsteady airfoil theory; although the panel code asymptotes to a slightly higher value of steady-state lift than the unsteady airfoil theory, this higher asymptotic value is a well-known effect of airfoil thickness. The second observation is that the experimental result matches the predictions of both inviscid models during the initial part of the run when the flap is in motion, but diverges from the theoretical predictions later in the run, after the flap has stopped moving and the lift builds to its steady-state value. The failure of the theory to predict the asymptotic experimental value of the steady-state lift is not surprising, since both Eq. (1) and the panel code are inviscid models. The good agreement between the inviscid models and the experimental results when the flap is in motion, although inferred from Drescher's[8] earlier work, is still an unexpected result, because, as shown in Fig. 3, there is an appreciable lowering of the static lift–curve slope, a viscous effect, over the range of flap deflection in the dynamic flap-motion experiment.

The close match between the experimental and inviscid model predictions during flap motion can be seen more clearly by comparing the detailed pressure histories of the experiment to those predicted using the unsteady panel code at corresponding instants during the motion. As was the case for removing the tare from the integrated C_n data, the individual pressure data was tared using the following approach. The tare for each transducer was defined as the difference between the experimentally measured C_p when the flap was not moving (at 0-deg flap deflection just prior to the start of the flap motion) and the C_p computed using a steady version of the panel code at the same tap location. Like the tare value used to adjust the C_n history, these C_p tares were calculated once using data at the start of the experiment when the flap was at a nominal steady deflection of 0 deg. For the experimental data of Fig. 4, a comparison of the experimentally measured C_p distribution and the panel-code computed C_p distribution for 0-deg flap deflection is given in Fig. 5a. The experimental pressure distributions for the entire experiment were then corrected by subtracting these constant C_p tares from the uncorrected C_p distributions at each subsequent measurement time. Note that, by choosing the panel code C_p distribution to be the true distribution at 0-deg flap deflection, the corrected C_p distribution was made to exactly match the panel code C_p distribution at the start of the experiment when the flap deflection was 0 deg. The behavior of the subsequent corrected C_p distributions with respect to this first distribution is, however, a representation of the dynamic behavior of the experimental data.

At the experimental scan rate of 300 data scans/s, a complete pressure distribution was acquired every 3.33 ms so that, during the 200 deg/s flap ramp to 10 deg, 15 complete pressure distributions were acquired while the flap was in motion. A comparison of 10 of these in-motion experimental pressure distributions (with tared C_p) to the predictions of the unsteady panel code is given in Figs. 5b–5k. These comparisons show that, prior to the onset of deceleration at approximately 8 deg, the computed, inviscid C_p distribution is nearly identical to the measured C_p distribution over the entire surface of the airfoil. Even after the motion begins deceleration, but prior to the cessation of motion, the comparison between computed and measured C_p distributions is still quite good as can be seen by examining Figs. 5i–5k. Figure 5k compares the distributions just as the flap deflection reached 10 deg at the end of the motion. If the agreement was good only in the region of the deflecting flap, one might conclude that noncirculatory effects produced local pressures similar to inviscid theory; however, good agreement of the pressure distributions over the entire airfoil can only be attained if both noncirculatory and circulatory effects are consistent between the experiment and the inviscid panel-code prediction. Plot 1 in Fig. 5 shows a comparison of the measured and computed airfoil pressure distributions approximately 35 clearing times ($V_\infty t/c = 35$) after the flap motion ended and the airfoil attained its near steady-state pressure distribution; at this point the distributions are in poor agreement over the entire airfoil surface. This poor agreement between experiment and the inviscid prediction for the static flap deflection is consistent with the measured static C_n given in Fig. 3 for $\delta_{TE} = 10$ deg.

D. Flap Ramps at Other Rates

The inviscid-like dynamic behavior of the moving flap was also observed in the data from flap–ramp experiments at nondimensional rates ranging from approximately 0.01 to 0.039 (the highest rate tested). As the nondimensional flap–ramp rate

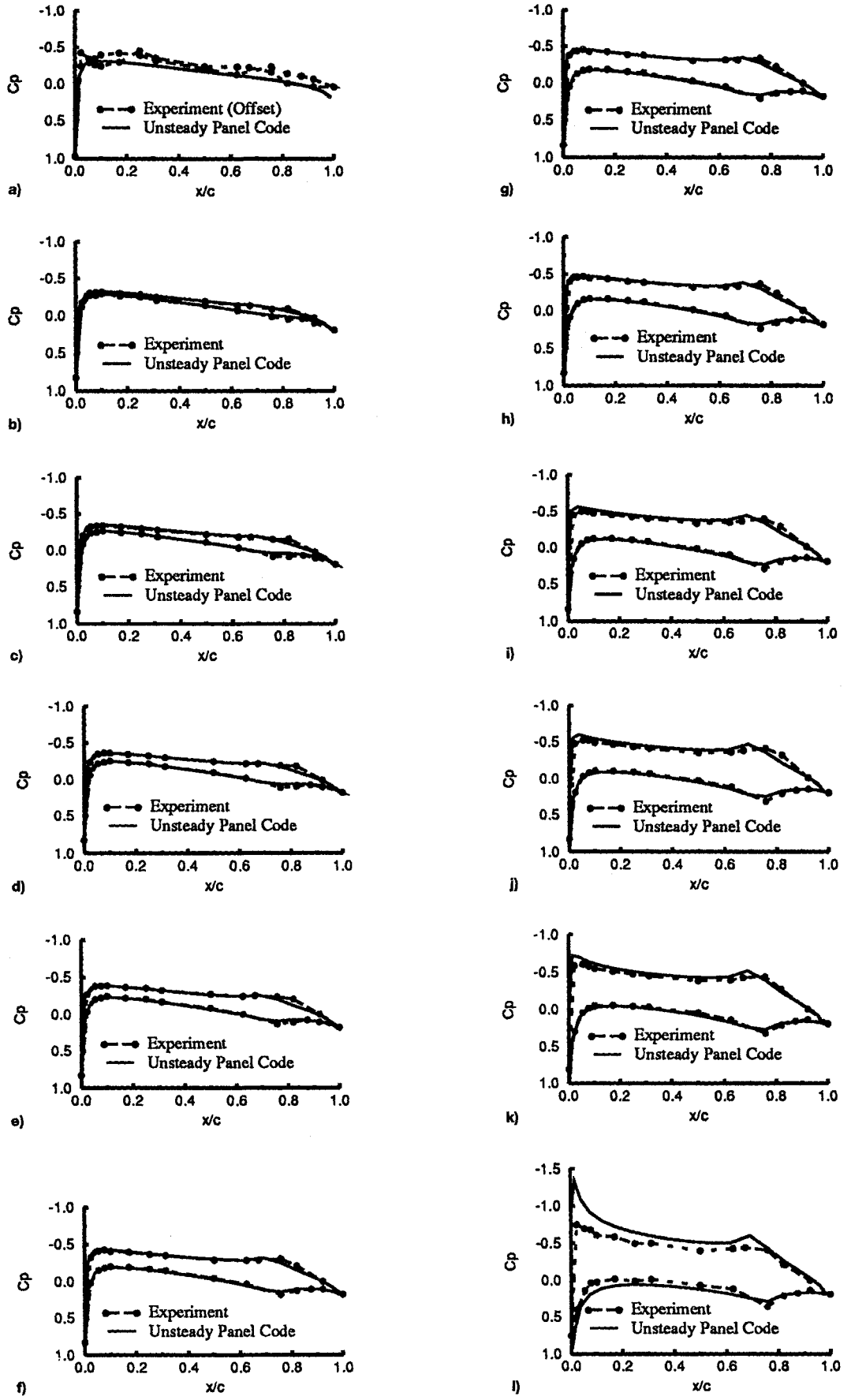

Fig. 5 Comparison of experimental C_p distributions with unsteady panel code: a) C_p offset ($\delta_{TE} = 0$ deg); b) $t = 0.108$ s, $\delta_{TE} = 1.25$ deg; c) $t = 0.115$ s, $\delta_{TE} = 2.67$ deg; d) $t = 0.118$ s, $\delta_{TE} = 3.43$ deg; e) $t = 0.122$ s, $\delta_{TE} = 4.19$ deg; f) $t = 0.128$ s, $\delta_{TE} = 5.75$ deg; g) $t = 0.132$ s, $\delta_{TE} = 6.45$ deg; h) $t = 0.135$ s, $\delta_{TE} = 7.12$ deg; i) $t = 0.142$ s, $\delta_{TE} = 8.53$ deg; j) $t = 0.145$ s, $\delta_{TE} = 9.08$ deg; k) $t = 0.158$ s, $\delta_{TE} = 10.0$ deg; and l) $t = 0.658$ s, $\delta_{TE} = 10.0$ deg.

decreased below 0.01, the lift response of the airfoil fell progressively below the inviscid predictions, until significant differences between experimental data and inviscid theory were observed at a nondimensional rate of 0.003. For the data in Fig. 4, a flap ramp from 0 to 10 deg, the inviscid-matching, higher effectiveness was sustained up to approximately 8 deg of flap deflection, the point where the ramp deceleration began. In other runs, for which the flap was ramped from 0 to 15 deg, the higher flap effectiveness was maintained to angles above 10 deg.

This inviscid-like performance during flap motion at nondimensional rates greater than 0.01 and reversion to steady, viscous performance once the flap decelerates and stops, appears to be consistent with the experiments of Drescher.[8] Close examination of Drescher's data reveals that his theoretical lift curves and pressure distributions, computed using inviscid unsteady airfoil theory, appear to match his experimental integrated pressure-lift curves through at least 10 deg of flap deflection at a nondimensional rate of 0.014 (e.g., see Fig. 33 of Ref. 8), and through at least 15 deg of flap deflection at a nondimensional rate of 0.048 (e.g., see Fig. 10 of Ref. 8). The *Re* for Drescher's experiment was 9×10^5, almost five times higher than the results reported here (although still far less than full-scale *Re*).

E. Angle-of-Attack Ramps

The previous observations of increased dynamic flap effectiveness led us to investigate whether angle-of-attack ramps would demonstrate a similar increase in lift–curve slope. Angle-of-attack ramp experiments were performed over a range in ramp angular rates of from 25 to 200 deg/s which, at the tunnel velocity of 45 ft/s, corresponded to nondimensional rates ($b\dot{\alpha}/V_\infty$) of from 0.003 to 0.026. The ramps were started from an initial angle of attack of 0 deg, and were of the same general form as the flap ramps.

The experimental airfoil C_n data were plotted against the prediction of unsteady airfoil theory in a manner similar to that for the dynamic flap ramp in Fig. 4. As in the case of the flap ramps, the airfoil C_n curves matched the inviscid theoretical prediction during the angle-of-attack ramps up to at least 7 deg, breaking away once the pitch motion ceased.[18,19] As for the flap–ramp cases, this characteristic suggests that the lift–curve slope $C_{l\alpha}$ for the airfoil is essentially equal to the theoretical inviscid value during the time the airfoil is pitching (upward or downward from $\alpha = 0$ deg).

F. Implications of Inviscid Dynamic Behavior on Unsteady Lift-Control Algorithm

The original purpose for these studies was to evaluate the extent to which unsteady airfoil theory could be employed in an algorithm designed to determine the trailing-edge flap motion required to control the unsteady lift on a pitching airfoil. In practice, all unsteady lift-control situations can be expected to have periods during which the trailing-edge flap moves at high nondimensional rates interspersed with periods during which the flap is either moving at low rates or is stationary. Thus, a control algorithm based solely on unsteady airfoil theory as given in Eq. (1) would not be appropriate. On the other hand, it is possible to identify the term in Eq. (1) that accounts for the discrepancy between the predictions and the experiment, once the motion has ceased.

It has been shown previously[17] that Eq. (1) converges to a value of steady-state lift determined by the coefficient a_4; thus, as time approaches infinity, Eq. (1) reduces to the following:

$$C_{l_{ss}} = a_4 \delta_{TE} \tag{4}$$

Equation (4) shows that the coefficient a_4 is directly related to τ[24]

$$a_4 = \tau C_{l\alpha} \eta = C_{l_{ss}}/\delta_{TE} \tag{5}$$

where η is an empirical correction for the effect of viscosity. Referring to Fig. 3, the steady value of a_4 should be 0.054/deg. If a_4 in Eq. (1) is changed from its theoretical, inviscid value of 0.0691/deg to the steady-state value of 0.054/deg and held constant over the entire experiment, only the asymptotic behavior of the data is matched, as can be seen by the fourth (lowest) curve in Fig. 4. Therefore, it can be concluded that the coefficient a_4 has varied over the course of the experiment.

It can be shown using indicial methods[5,7,19,27,28] that the appropriate form of Eq. (1) that allows for changes in a_4 (either abrupt or otherwise) is given by

$$C_l = a_1 \dot{\delta}_{TE} + a_2 \ddot{\delta}_{TE} + \int_0^s \left[\frac{d(a_4 \delta_{TE})}{d\sigma} + a_3 \ddot{\delta}_{TE} \right] \phi(s - \sigma)\, d\sigma \tag{6}$$

the difference between Eq. (6) and Eq. (1) being the inclusion of a_4 inside the derivative with respect to nondimensional time. It is possible to essentially duplicate the experimental curve in Fig. 4 by using Eq. (6) with a_4 equal to 0.0691/deg while the flap is in motion and decreasing to 0.054/deg over a few clearing times once the motion ceases. The ability to predict the experimental behavior in this way suggests that viscous effects, not accounted for in Eq. (1), can be handled by appropriate modifications in flap effectiveness through changes of a_4, in Eq. (6).

G. Physical Rationale for Motion-Enhanced Flap Effectiveness

The fact that in steady flow the lift, or pressure distribution (Fig. 5l), is deficient compared to the theoretical results can be attributed to viscous effects,[24] that is, the flow is never fully conforming to the airfoil in the trailing-edge region because of the boundary-layer and/or partially separated flow. These conditions lead to finite, momentum-deficit wakes and a nonrigorous enforcement of the Kutta condition. This relaxed Kutta condition affects the pressure distribution around the entire airfoil, leading to a reduction in lift below that predicted by inviscid theory. In an attempt to observe whether the flap motion affected the trailing-edge flow pattern in our experiments, flow visualization studies were performed around the trailing edge of the airfoil during both static and dynamic flap deflections. Figures 6a and 6b show kerosene smoke flow visualization[29] around the flap at a deflection of 10 deg, when the flap is fixed at 10 deg (Fig. 6a) and when the flap is dynamically passing through 10 deg (during a ramp to 15 deg) at a nondimensional rate of 0.02 (Fig. 6b). The comparisons show that the flow is more conforming to the surface of the flap in the dynamic case. Also, the wake is narrower in the dynamic case and the upper (outer) streamlines (streaklines) are curved downward in the dynamic case. These findings are in accordance with those of Drescher,[8] who noted a persistence

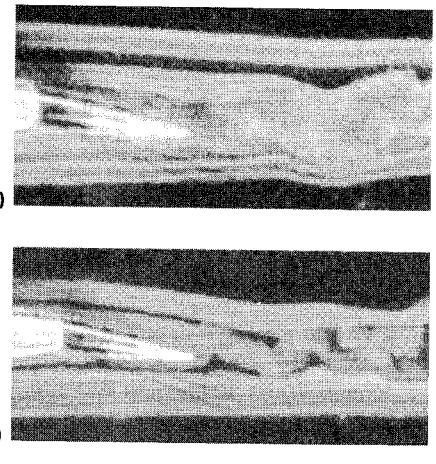

Fig. 6 Visualization of flow around trailing-edge flap (deflection = 10 deg): a) static and b) dynamic.

of the attached flow state during similar dynamic flap–ramp flow visualization experiments.

That such flap-surface flow conformity leads to increased effectiveness has been experimentally verified for steady flows. As reported in Ref. 30, Arnold showed that the theoretical inviscid flap effectiveness was achieved when sufficient suction was applied at the flap to just prevent separation of the boundary layer. It has been shown that airfoil dynamic pitch motions can suppress separation,[31] and that airfoil motion in some cases can be directly compared with suction.[32] Thus, the fact that separation has been seen to be suppressed over the flap when the flap is in motion is not wholly unexpected. These visualization experiments are consistent with the comparisons of Fig. 5, and tend to support the modifications to a_4 in Eq. (6).

IV. Lift-Control Results

As a demonstration of the significance of rate-dependent flap effectiveness on an unsteady lift-control algorithm based on unsteady airfoil theory, experimental lift-control results are presented here in which the trailing-edge flap control motion was computed using Eq. (6) with the flap effectiveness fixed alternatively at the inviscid value (a_4 = 0.0691/deg), at the static value (a_4 = 0.054/deg) for the entire experiment, and transitioning during the experiment from the inviscid value to the static value at the cessation of flap motion.

For the experimental unsteady lift-control results shown here, an attempt was made to use the trailing-edge flap to cancel (control to zero lift) the lift associated with a pitch-up motion of the airfoil about its midchord from 0- to 7-deg angle of attack at a nondimensional pitch rate ($\dot{\alpha}b/V_\infty$) of 0.01. The first curve in Fig. 7 shows the airfoil's experimental lift history in the absence of any control. Curve 2 shows the airfoil's experimental lift history with the trailing-edge flap driven as prescribed by the lift-control algorithm in which the flap effectiveness was kept constant and equal to the inviscid value (i.e., a_4 = 0.0691/deg). Curve 3 shows the airfoil's lift history with the flap schedule determined assuming that the effectiveness was constant and equal to the measured steady value (a_4 = 0.054/deg). The final curve, curve 4, gives the lift history with the flap motion determined assuming that the effectiveness was equal to the inviscid value while the flap was in motion, and equal to the measured steady value after the motion stopped. Referring to Fig. 3, it should be noted that the slight nonlinearity in the flap lift–curve slope for negative deflection angles greater than −10 deg has been taken into account in the final lift-control experiment; this accounts for the fact that the final curve asymptotes to a steady C_n of zero, while the curve for which a_4 was kept constant at 0.054/deg asymptotes to a steady C_n slightly greater than zero. For curve 4, a smooth cosine function was used to transition from the higher to the lower effectiveness between the times of 0.23–0.3 s (3.5 airfoil clearing times). Figure 7 shows that the lift is controlled reasonably well using the inviscid effectiveness as long as the flap is in motion, while use of the measured, steady effectiveness results in a flap motion that overcontrols the lift (i.e., actually produces negative lift) during the motion. The best control of the lift is obtained when the flap effectiveness is transitioned from the higher to the lower effectiveness after the motion is completed (curve 4).

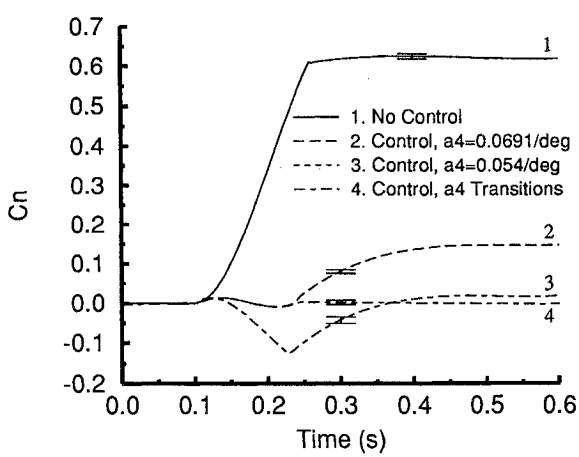

Fig. 7 Lift control of angle-of-attack ramp to 7 deg.

V. Conclusions

The flap effectiveness was found to be higher during motion than in the steady case. Results obtained showed that a transition in flap effectiveness was required to control the motion-induced lift to zero. The flow visualization studies clearly indicate that the motion enhancement of effectiveness is associated with viscous phenomena. Based on our low Reynolds number experiments, it is inappropriate to conclude that similar phenomena are present for full-scale systems; however, lift–curve slopes for high Reynolds number airfoils and flaps in steady flow are close to those reported here. Because of the control ramifications to full-scale aircraft, it seems imperative that similar experiments should be performed at higher Reynolds number.

Acknowledgments

This work was supported by the University of Notre Dame, Department of Aerospace and Mechanical Engineering, and in its early stages by the McDonnell Douglas Corporation. We are appreciative of the technical support provided by Richard E. Boalbey and Wayne Ely of McDonnell, and Ronald J. Hugo of the University of Notre Dame. We would also like to thank Michael Swadener and Joel Preston for their invaluable assistance in constructing the test section and instrumentation. Computational resources were provided by the IBM-SUR program.

References

[1]Lang, J. D., and Francis, M. S., "Unsteady Aerodynamics and Dynamic Aircraft Maneuverability," *Proceedings of the AGARD Symposium, Unsteady Aerodynamics—Fundamentals and Applications to Aircraft Dynamics* (Göttingen, Germany), AGARD, 1985.

[2]Jumper, E. J., Schreck, S. J., and Dimmick, R. L., "Lift-Curve Characteristics for an Airfoil Pitching at Constant Rate," *Journal of Aircraft*, Vol. 25, No. 10, 1987, pp. 680–687.

[3]Skow, A. M., "Agility as a Contributor to Design Balance," *Journal of Aircraft*, Vol. 29, No. 1, 1992, pp. 34–46.

[4]Theodorsen, T., "General Theory of Aerodynamic Instability and the Mechanism of Flutter," NACA TR 496, 1935.

[5]Jones, W. P., "Aerodynamic Forces on Wings in Non-Uniform Motion," British Aeronautical Research Council, R&M 2117, Aug. 1945.

[6]Küssner, H. G., and Schwarz, I., "The Oscillating Wing with Aerodynamically Balanced Elevator," NACA TM 991, 1941.

[7]Leishman, J. G., "Unsteady Lift of a Flapped Airfoil by Indicial Concepts," *Journal of Aircraft*, Vol. 31, No. 3, 1994, pp. 288–297.

[8]Drescher, H., "Untersuchungen an einem symmetrischen Tragflugel mit spaltlos angeschlossenem Ruder bei raschen Aenderungen des Ruderausschlags (ebene Stromung)," *Mitt. Max-Planck-Inst. Strömungs-Forsch.* Nr. 6, Göttingen, Germany, 1952.

[9]Zwaan, R. J., "NACA 64A006 Oscillating Flap," *A Compendium of Unsteady Aerodynamic Measurements*, edited by N. C. Lambourne, AGARD R-702, 1980.

[10]Zwaan, R. J., "NLR 7301 Supercritical Airfoil—Oscillatory Pitching and Oscillating Flap," *A Compendium of Unsteady Aerodynamic Measurements*, edited by N. C. Lambourne, AGARD R-702, 1980.

[11]Edwards, J. W., "Active Flutter Control Using Generalized Unsteady Aerodynamic Theory," *Journal of Guidance and Control*, Vol. 1, Jan. 1978, pp. 32–40.

[12]Edwards, J. W., "Flight Test Results of an Active Flutter Suppression System," *Journal of Aircraft*, Vol. 20, No. 3, 1983, pp. 267–274.

[13]Karpel, M., "Design for Active Flutter Suppression and Gust Alleviation Using State-Space Aeroelastic Modeling," *Journal of Air-*

craft, Vol. 19, No. 3, 1982, pp. 221–227.

[14]Murrow, H. N., and Eckstrom, C. V., "Drones for Aerodynamic and Structural Testing (DAST)—A Status Report," *Journal of Aircraft*, Vol. 16, No. 8, 1979, pp. 521–526.

[15]Hwang, C., Winther, B. A., and Mills, G. R., "Demonstration of Aircraft Wing/Store Flutter Suppression Systems," *Journal of Aircraft*, Vol. 16, No. 8, 1979, pp. 557–563.

[16]Nixon, D., and Tzuoo, K. L., "Prediction of Gust Loadings and Alleviation at Transonic Speeds," *Journal of Aircraft*, Vol. 24, No. 10, 1987, pp. 703–709.

[17]Hugo, R., and Jumper, E., "Controlling Unsteady Lift Using Unsteady Trailing-Edge Flap Motions," AIAA Paper 92-0275, Jan. 1992.

[18]Rennie, R. M., and Jumper, E. J., "Experimental Measurements of Dynamic Control Surface Effectiveness," AIAA Paper 94-0504, Jan. 1994.

[19]Rennie, R. M., "An Experimental Investigation of Unsteady Lift Control Using Trailing-Edge Flaps," Ph.D. Dissertation, Dept. of Aerospace and Mechanical Engineering, Univ. of Notre Dame, Notre Dame, IN, April 1996.

[20]McCroskey, W. J., Carr, L. W., and McAllister, K. W., "Dynamic Stall Experiments on Oscillating Airfoils," *AIAA Journal*, Vol. 14, No. 1, 1976, pp. 57–63.

[21]Carta, F. O., and Lorbert, P. F., "Experimental Study of the Aerodynamics of Incipient Torsional Stall Flutter," *Journal of Propulsion*, Vol. 3, No. 3, 1987, pp. 164–170.

[22]Batill, S. M., and Nebres, J. V., "Application of Digital Filtering Techniques to Unsteady Pressure Measurements," AIAA Paper 91-0061, Jan. 1991.

[23]Rae, W. H., and Pope, A., *Low-Speed Wind Tunnel Testing*, Wiley, New York, 1984.

[24]McCormick, B. M., *Aerodynamics, Aeronautics, and Flight Mechanics*, Wiley, New York, 1979.

[25]Hess, J. L., and Smith, A. M. O., "Calculations of Potential Flow About Arbitrary Bodies," *Progress in Aeronautical Sciences*, Vol. 8, 1967, pp. 1–139.

[26]Basu, B. C., and Hancock, G. J., "The Unsteady Motion of a Two-Dimensional Aerofoil in Incompressible Inviscid Flow," *Journal of Fluid Mechanics*, Vol. 87, Pt. 1, 1978, pp. 159–178.

[27]Leishman, J. G., "Validation of Approximate Indicial Aerodynamic Functions for Two-Dimensional Subsonic Flow," *Journal of Aircraft*, Vol. 25, No. 10, 1988, pp. 914–922.

[28]Meirovitch, L., *Introduction to Dynamics and Control*, Wiley, New York, 1985, pp. 23, 24.

[29]Batill, S. M., Nelson, R. C., and Mueller, T. J., "Smoke Flow Visualization at Transonic and Supersonic Mach Numbers," AIAA Paper 82-0188, Jan. 1982.

[30]Schlichting, H., and Truckenbrodt, E., *Aerodynamics of the Airplane*, McGraw–Hill, New York, 1979.

[31]Daley, D. C., and Jumper, E. J., "Experimental Investigation of Dynamic Stall for a Pitching Airfoil," *Journal of Aircraft*, Vol. 21, No. 10, 1984, pp. 831, 832.

[32]Jumper, E. J., "Mass Ingestion: A Perturbation Method Useful in Analyzing Some Boundary-Layer Problems," American Society of Mechanical Engineers Paper 86-WA/FE-10, Dec. 1986.